Precision Spectroscopy of the Fine and Hyperfine Structures of High Molecular Rydberg-Stark States: Metrology of Molecular Hydrogen Ions

I. Doran,[1] L. Jeckel,[1] M. Beyer,[2] Ch. Jungen,[3] and F. Merkt[1,4,5,*]
[1]Institute of Molecular Physical Science, ETH Zürich, 8093 Zürich, Switzerland
[2]Department of Physics and Astronomy, LaserLaB, Vrije Universiteit Amsterdam, de Boelelaan 1081, 1081 HV Amsterdam, The Netherlands
[3]Université Paris-Saclay, Centre National de la Recherche Scientifique, Laboratoire Aimé Cotton, 91400 Orsay, France
[4]Department of Physics, ETH Zürich, Zürich, Switzerland
[5]Quantum Center, ETH Zürich, Zürich, Switzerland

(Received 24 February 2026; revised 13 May 2026; accepted 8 July 2026; published 7 August 2026)

The Stark effect in autoionizing high-n Rydberg states decouples the Rydberg electron from the ion core through ℓ mixing with core-nonpenetrating high-ℓ states. The Rydberg states become long-lived, which is ideal for precision spectroscopy, and their structures reflect the fine and hyperfine structures of the ion-core levels. We report on precision measurements, in weak electric fields, of the fine and hyperfine structures of two distinct categories of high autoionizing molecular Rydberg-Stark states differing by the nature of the ion-core angular momentum: Rydberg states of *para*-H_2 (total nuclear spin $I = 0, 2$) with a rotationally excited ($N^+ = 2$) H_2^+ ion core and Rydberg states of *ortho*-D_2 ($I = 0, 2$) with a rotationless ($N^+ = 0$) ion core. The spectra reveal striking differences which are interpreted as arising from the dominance of anisotropic charge-quadrupole interactions between the rotating quadrupolar ion core and the Rydberg electron in *para*-H_2 and the absence of such interactions in rotationless *ortho*-D_2 Rydberg states. In *ortho*-D_2, the dominant interaction, the magnetic Fermi-contact hyperfine interaction in the ion core, does not significantly affect the motion of the Rydberg electron. By analyzing these spectra based on a treatment combining multichannel quantum-defect theory and matrix diagonalization, we derive new experimental values of the hyperfine coupling constant $b_F = 139.84(5)$ MHz of $D_2^+(v^+ = 1, N^+ = 0)$, the spin-rotation coupling constant $c_e = 39.62(11)$ MHz of $H_2^+(v^+ = 1, N^+ = 2)$ and the fundamental vibrational interval of *ortho*-D_2^+ [47 279 980.8(1.9) MHz]. The approach followed here in the study of molecular Rydberg-Stark states is general and broadly applicable to measurements of the fine and hyperfine structures of molecular cations.

DOI: 10.1103/5rsv-mb6x

We report on precision measurements of the spectra of highly excited electronic states (Rydberg states) of the two-electron molecules H_2 and D_2 in the presence of external electric fields. In these states, the molecules can be regarded as consisting of an H_2^+ or D_2^+ ion core and a weakly bound electron moving in distant orbits corresponding to large values of the principal quantum number n, as illustrated schematically in Fig. 1. Even weak electric fields induce a large Stark effect in these states and strongly modify their structure and dynamics [1,2]. The measurements aim at characterizing all interactions in these highly excited states, including those involving the magnetic and electric moments of the nuclei (leading to the hyperfine structure), the ion-core molecular rotation and the spin and orbital motions of the excited electron (leading to the fine structure).

The precise characterization of the structure and dynamics of simple, few-body atomic and molecular systems is of intrinsic fundamental interest, and also increasingly used to improve the values of fundamental constants, test fundamental physical theories and search for physics beyond the standard model of particle physics [3–12]. Current efforts are also invested toward exploiting high atomic and molecular Rydberg-Stark states in electric-field quantum sensing [13–15] and quantum-information processing [16–20]. Rydberg states exhibiting hyperfine structures are attractive systems in this context because nuclear spins can be exploited to enhance the efficiency of quantum gates and quantum-information-processing protocols [21].

The Stark effect in high atomic and molecular Rydberg states is particularly strong in energy regions near zero-quantum-defect positions, where $\ell \geq 4$ states are almost degenerate (ℓ is the Rydberg-electron orbital-angular-momentum quantum number). The Stark shifts are linear even at low field strengths [1,2,22] and the level structure fans out with increasing field strength $\mathcal{F}$ in linear manifolds

*Contact author: frederic.merkt@phys.chem.ethz.ch

 © 2026 American Physical Society

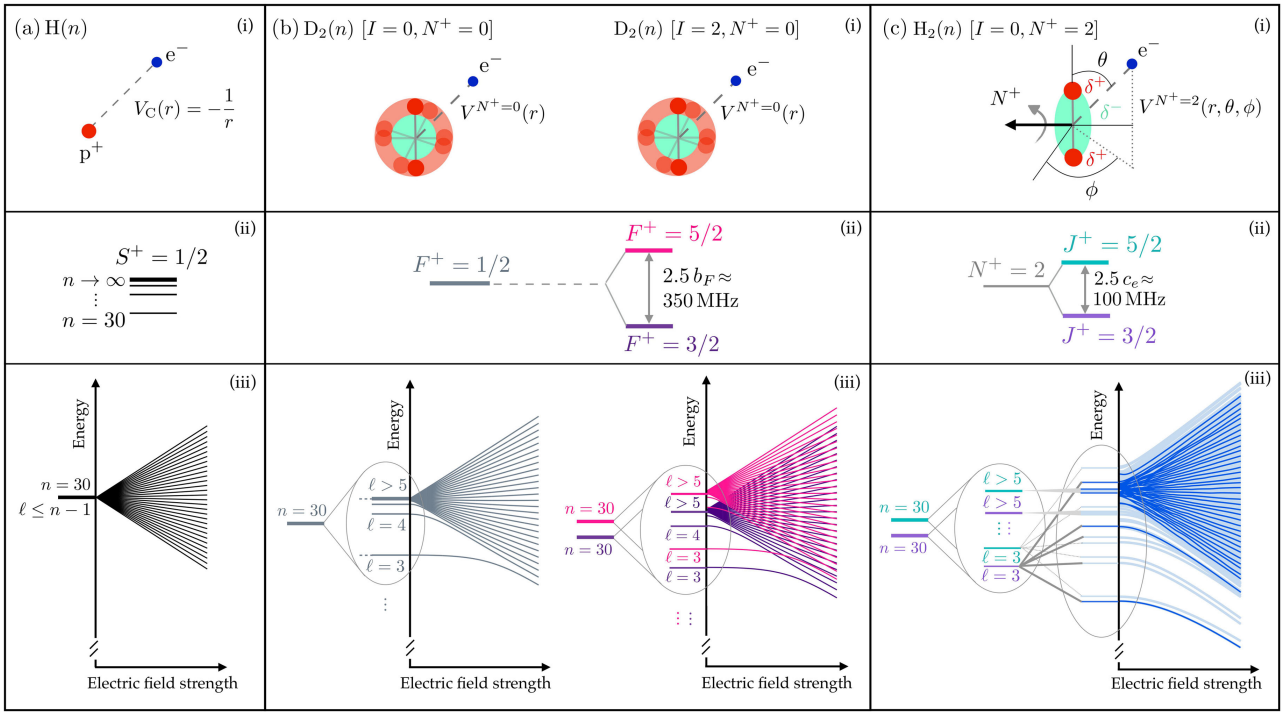


FIG. 1. Schematic illustration of the salient features of the Stark effect in Rydberg states of (a) the H atom with a pointlike H^+ ion core and a pure Coulomb potential $V_C(r)$, (b) *ortho*-D_2 with an $N^+ = 0$ ion core and a central potential $[V^{N^+=0}(r)]$ deviating at short range from a Coulomb potential. Left: $I = 0$; right: $I = 2$ (with core hyperfine structure), and (c) *para*-H_2 with $N^+ = 2$ with spin-rotation splitting and a quadrupolar ion core causing an anisotropic long-range charge-quadrupole interaction $V^{N^+=2}(r,\theta,\phi)$. (i) Rydberg-electron–ion-core interactions. The ion-core quadrupole is indicated schematically by the partial charges and their color code in (b) and (c). (ii) Ion-core level structure. (iii) Rydberg-level structure at $n = 30$ and its field dependence. See text for details.

of Stark states, see Fig. 1. The Stark states are labeled with an index k ranging from $-(n - |m| - 1)$ to $(n - |m| - 1)$ in steps of 2. The linear Stark shifts are $3nk\mathcal{F}/2$ (in atomic units), giving rise to characteristic patterns of equidistant states [1,2,22]. The electric field decouples the Rydberg electron from the ion core by inducing ℓ mixing with long-lived core-nonpenetrating high-ℓ Rydberg states ($\ell \geq 4$). Three advantages result for precision spectroscopy: (i) the Rydberg states become long-lived and the autoionization resonances sharp, (ii) the ion-core level structure can be deduced from the structure of the Rydberg-Stark states [23], and (iii) ℓ mixing provides access to multiple Rydberg series and to a global understanding of their structure and dynamics.

In Rydberg states of atoms with closed-shell ion cores, the Stark effect can be accurately treated by matrix-diagonalization procedures [24–28]. These procedures can be extended to Rydberg atoms with open-shell ion cores (see Refs. [29–32] for early examples) and molecules [33–39]. Alternative treatments of the Stark effect based on multichannel quantum-defect theory have also been developed [40–47]. The understanding of the Stark effect in Rydberg states is thus satisfactory, with one important exception: no experimental data have been reported yet on molecular Rydberg-Stark states at a sufficiently high resolution to reveal their hyperfine structures. This gap is filled in the present Letter.

When the ion core exhibits coupled electronic (Λ^+, Ω^+), rotational (N^+), electron-spin (S^+), and nuclear-spin (I) degrees of freedom, the rigorous treatment of the Stark effect necessitates the systematic use of angular-momentum tensor algebra and elaborate representations of complex angular-momentum coupling hierarchies [48]. These hierarchies evolve rapidly with n and ℓ and are strongly modified through ℓ mixing by external electric fields. We have recently developed a new approach [49] combining multichannel quantum-defect theory [50,51] and matrix diagonalization [24] to accurately calculate the fine and hyperfine structures of molecular Rydberg-Stark states with open-shell ion cores. To test this approach, we present here studies of two categories of Rydberg-Stark states of H_2 and D_2 with ion cores in the first vibrationally excited state ($v^+ = 1$) of the ground $X^+\ ^2\Sigma_g^+$ electronic state. These states decay by autoionization to the available continua. However, the rapid autoionization of low-ℓ Rydberg states is suppressed in Stark states by field-induced ℓ mixing, which is crucial for the observation of their fine and hyperfine structures. A schematic representation and a comparison with the more familiar situation encountered in the H atom is presented in Fig. 1.

The first category [Fig. 1(b)] concerns Rydberg states of *ortho*-D_2 ($I = 0$, 2) with a rotationless ($N^+ = 0$) D_2^+ ion core. The D_2^+ ion core splits into one $I = 0, S^+ = F^+ = 1/2$ component and two $I = 2$ hyperfine components with $F^+ = 3/2$ and $F^+ = 5/2$, separated by $2.5b_F$ [52]. The second category [Fig. 1(c)] concerns Rydberg states of *para*-H_2 ($I = 0$) with an $N^+ = 2$ H_2^+ ion core, which splits into two ($J^+ = 3/2$ and $J^+ = 5/2$) fine-structure (spin-rotation) components separated by $2.5c_e$ [53] [Fig. 1(c)]. The top part of Fig. 1 illustrates the interaction of the Rydberg electron with (a) a proton, (b) a nonrotating (i.e., spherically symmetric) quadrupolar and polarizable molecular ion core, and (c) a rotating quadrupolar and polarizable molecular ion core. The middle parts (ii) depict the ion-core level structures, and the bottom parts (iii) show the level structures of the Rydberg states with (right) and without (left) field.

The $I = 0$ states in *ortho*-D_2 enable the direct comparison with atomic hydrogen [Fig. 1(a)] and the identification, by comparison with the $I = 2$ nuclear-spin-symmetry species, of the effects arising from the hyperfine structure. In both categories [see Figs. 1(b) and 1(c)], the ion core comprises a single angular momentum [$N^+ = 2$ in the case of H_2^+ ($I = 0$) and $I = 2$ in the case of D_2^+ ($N^+ = 0$)] in addition to the core-electron spin. These systems turned out to be ideal to validate our new computational approach [49] and enabled the observation of phenomena not anticipated at the outset of the investigation: (i) strikingly different spectral patterns in H_2 and D_2, which could be interpreted during the analysis, and (ii) different autoionization dynamics of different hyperfine components of specific Stark states in D_2, which remains unexplained. These systems were also ideal to demonstrate the possibility of precisely determining the fine and hyperfine structures of molecular ions from Rydberg-Stark spectra.

The experimental procedure relies on the zero-quantum-defect method [23,54] and the experimental setup described in Refs. [23,55]. In brief, Rydberg states converging to the ($v^+ = 1, N^+ = 0$) and ($v^+ = 1, N^+ = 2$) levels of the $X^+\,{}^2\Sigma_g^+$ electronic ground state of D_2^+ and H_2^+, respectively, are accessed from the ($v = 2$, $N = 2$) and ($v = 2$, $N = 0$) levels of the $GK\,{}^1\Sigma_g^+$ double-minimum electronically excited state of H_2 and D_2 using cw single-mode near-infrared (NIR) laser radiation. These GK levels are prepared by resonant two-photon excitation from the ground state using pulsed vacuum-ultraviolet and visible laser radiation (repetition rate 25 Hz, pulse duration ≈5 ns) [55]. To minimize Doppler broadening and shifts, a doubly skimmed supersonic beam emitted from a cryogenic pulsed valve is crossed at near-right angles by the NIR laser beam. Retroreflection of this laser beam gives rise to two Doppler components with opposite Doppler shifts, which are averaged to obtain the first-order-Doppler-free transition frequencies [55]. To avoid spectral congestion, the final measurements are carried out after blocking the retroreflected NIR laser beam. The frequency calibration is performed using a frequency comb (Menlo Systems, FC1500-250-WG) referenced to a 10 MHz Rb GPS standard, see Ref. [55]. The photoexcitation region is surrounded by a magnetic shield to reduce stray magnetic fields to below 2×10^{-7} T. To record Stark spectra, weak (< 150 V/m) homogeneous electric fields $\mathcal{F}$ in the photoexcitation region are generated by applying dc electric potentials $V_{\rm dc}$ across a stack of cylindrical electrodes [55]. This stack is also used to apply large pulsed electric potentials $V_{\rm extr}$, typically ≈1 μs after photoexcitation, to extract the ions produced following autoionization of the Rydberg-Stark states toward a microchannel-plate detector. Spectra are recorded by monitoring the autoionization yield as a function of the NIR laser frequency.

To characterize the Stark effect and derive ionization energies and the ion fine and hyperfine structures, we measured spectra between $n \approx 30$ and 45 and field strengths between ≈70 and 150 V/m for Rydberg states converging to both D_2^+ $X^+(1,0)$ and H_2^+ $X^+(1,2)$, see Tables SI and SII of Supplemental Material [56]. Figure 2 shows, as illustrations, Stark spectra of $n = 34$ Rydberg-Stark states of D_2 (a) and H_2 (b). Both spectra reveal a complex structure, reflecting the fine and hyperfine structures. In the D_2 spectrum, each Stark state (k) appears as a triplet that exactly matches the hyperfine structure of the ion core, see Fig. 1(b)(ii), as indicated with the colored assignment bars in Fig. 2(a)(ii) for k values between −3 and 7. In analogy, one would expect the Stark states in the case of H_2 to split into two manifolds associated with the $N^+ = 2, J^+ = 3/2$, and $5/2$ spin-rotation components of the ion core, see Fig. 1(c)(ii). This is not the case: the H_2 spectrum consists of at least three distinct progressions [see Fig. 2(b)(ii)]. In selected regions, the fine-structure splittings match the ion-core spin-rotation intervals, as indicated by the colored doublets in Fig. 2(b)(ii), whereas in other regions no splittings corresponding to the ion-core spin-rotation interval are observable at all, see, e.g., the region around −2200 MHz in Fig. 2(b)(i). The H_2 spectrum is less regular than the D_2 spectrum despite the fact that the H_2^+ and D_2^+ ion cores each exhibit only one type of angular momentum ($I = 2$ for D_2 and $N^+ = 2$ for H_2) beside the core-electron spin.

To understand the origin of this difference and assign the spectra, the Stark effect was calculated by diagonalizing the matrix of the total effective Hamiltonian $\hat{H} = \hat{H}_0 + e\mathcal{F}\hat{z}$ [24] consisting of the zero-field Hamiltonian $\hat{H}_0$ and the interaction $e\mathcal{F}\hat{z}$ with the external field. The elements of $\hat{H}_0$ correspond to the zero-field energies depicted in Figs. 1(b)(iii) and 1(c)(iii) and were determined using multichannel quantum-defect-theory (MQDT) calculations for $\ell \leq 3$ Rydberg states and a long-range interaction model accounting for both electrostatic and hyperfine interactions for $\ell \geq 4$ Rydberg states [49]. The matrix elements of $e\mathcal{F}\hat{z}$ were evaluated using angular-momentum tensor algebra [49] and lead to the Stark manifolds depicted schematically in Figs. 1(b)(iii) and 1(c)(iii). Because the intermediate GK

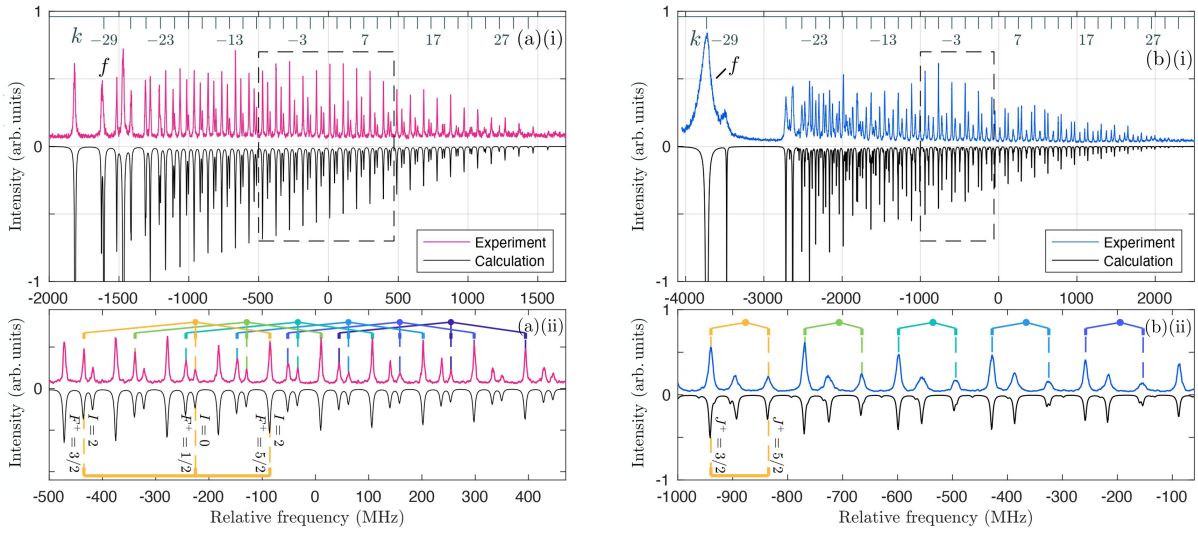


FIG. 2. Measured spectra of the $n = 34$ [(a) D_2^+ $X^+(1,0)$ and (b) H_2^+ $X^+(1,2)$] Rydberg-Stark manifolds at electric fields of 69.79 and 124.35 V/m, respectively, as determined from fits, and calculated spectra (inverted traces) assuming line widths of 5 MHz for all lines. Selected spectral regions [delimited by dashed lines in panels (i)] are enlarged in panels (ii). See text.

state has dominant singlet d ($S = 0, \ell = 2$) character, the transition intensities are in good approximation proportional to the singlet f ($S = 0, \ell = 3$) character of the Rydberg-Stark states.

Agreement between measured and calculated (inverted traces in Fig. 2) spectra was reached in a fit of the ionization energies [i.e., the D_2^+ X^+ (1,0)–D_2 GK(2,2) and H_2^+ X^+ (1,2)–H_2 GK(2,0) intervals], the electric field strengths [69.79(3) and 124.35(3) V/m for D_2 and H_2, respectively], as well as the Fermi-contact hyperfine coupling constant b_F in the case of D_2^+ $X^+(1,0)$ and the spin-rotation coupling constant c_e in the case of H_2^+ $X^+(1,2)$ (see Table I for the final results). The calculated line positions reproduce the experimental ones well, with weighted rms fit values below 5. The intensities are also well reproduced, particularly on the high-frequency side. On the low-frequency side, saturation of the transitions and lifetime broadening of states with large f character lead to reduced experimental peak intensities, see, e.g., the line labeled "f" in the H_2 spectrum.

TABLE I. Hyperfine (spin-rotation) coupling constants b_F (c_e) in *ortho*-$D_2^+(v^+ = 1, N^+ = 0)$ [*para*-$H_2^+(v^+ = 1, N^+ = 2)$] and ionization energies D_2^+ $X^+(1,0)$–D_2 GK(2,2) [H_2^+ $X^+(1,2)$–H_2 GK(2,0)] and their uncertainties.

Energy interval	Value (MHz)
b_F [$D_2^+(v^+ = 1, N^+ = 0)$] (Exp[a])	139.84(5)
b_F [$D_2^+(v^+ = 1, N^+ = 0)$] (Th[b])	139.837(10)
D_2^+ $X^+(1,0)$-D_2 GK(2,2) (Exp[a])	393 751 511.3(3)
c_e [H_2^+ $X^+(1,2)$] (Exp[a])	39.62(11)
c_e [H_2^+ $X^+(1,2)$] (Th[c])	39.5716
H_2^+ $X^+(1,2)$–H_2 GK(2,0) (Exp[a])	401 128 310.3(3)

[a]From this Letter.
[b]From Ref. [52].
[c]From Ref. [53].

The autoionization of the high-k Rydberg-Stark states of D_2^+, which have the smallest contributions from short-lived low-ℓ states, was slow enough to lead to a tail in the D_2^+ time-of-flight distributions. Figure 3 compares spectra obtained by recording the D_2^+ ion signal corresponding to the tail (a) and the main signal (b) and their ratio (c). The comparison reveals that the $I = 0$ Rydberg-Stark states [blue dots in Fig. 3(c)] autoionize faster than the $I = 2$ Rydberg-Stark states (green and orange dots for $F^+ = 3/2$ and 5/2, respectively). This dependence of the autoionization on I is not accounted for by the calculations because the MQDT parameters used in the model are the same for $I = 0$ and 2.

Given the otherwise very good agreement between calculated and measured spectra (see Fig. 2), the calculations can be used to explain the different behaviors observed in H_2 and D_2. The calculated zero-field level structures at $n = 30$ are depicted schematically in Figs. 1(a)(iii), 1(b)(iii), and 1(c)(iii). The different ℓ levels are almost degenerate at zero field in the H atom [28,57] [thick black bar in Fig. 1(a)(iii)]. The Stark effect is thus almost perfectly linear. In D_2, the zero-field levels extend over a broader spectral region [gray and colored horizontal lines in Fig. 1(b)(iii)] because of the deviations from a pure Coulomb potential resulting from the charge distribution and the isotropic polarizability of the $N^+ = 0$ ion core. These deviations rapidly decrease with increasing ℓ values. The Stark effect is similar to that of the H atom, with the main difference that the low-ℓ levels are subject to a quadratic Stark shift at low fields. The calculations reveal a negligible coupling of the nuclear ($I = 2$) and core-electron

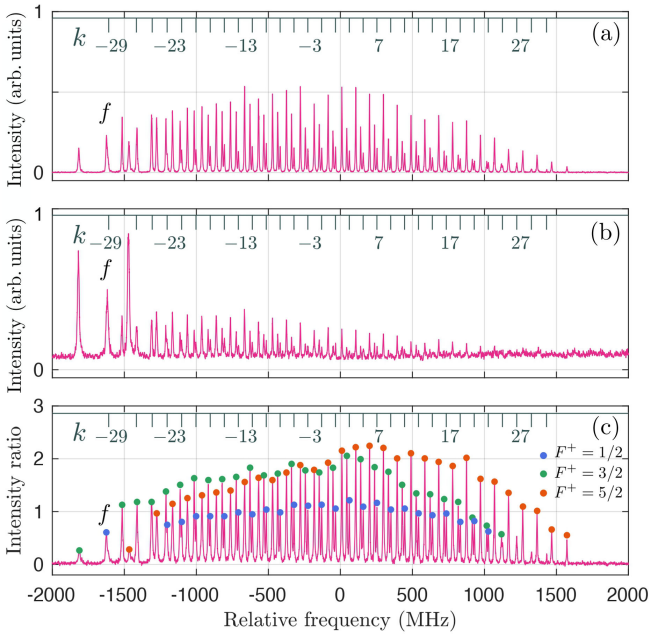


FIG. 3. Spectra of the $n = 34$ [D_2^+ $X^+(1,0)$] Rydberg-Stark manifolds at electric field strengths of 69.79 V/m measured in the (a) slow and (b) fast-autoionization time-of-flight windows. (c) Ratio of the spectra in panels (a) and (b). The assignment bars give the value of k.

($S^+ = 1/2$) spins with the Rydberg electron orbital and spin angular momenta at high n. As a result, the Rydberg electron motion is almost perfectly separable from the core motion that is dominated by the hyperfine interaction. Consequently, the Rydberg-level structure is a superposition of three separate and almost identical manifolds for the $I = 0, F^+ = 1/2$ [gray in Fig. 1(b)(iii)], $I = 2; F^+ = 3/2$ (violet) and $I = 2; F^+ = 5/2$ (pink) core states, as observed in Fig. 2(a).

In H_2 ($N^+ = 2$), additional zero-field splittings arise from the anisotropic core polarizability and the interaction between the electron and the ion-core quadrupole moment, which do not average out for $N^+ \geq 1$ rotational levels [compare zero-field structures in Figs. 1(b)(iii) and 1(c)(iii)]. In this case, the core rotational angular momentum $\vec{N}^+$ is coupled to both the ion-core electron spin $\vec{S}^+$ via the spin-rotational interaction and the Rydberg-electron orbital angular momentum $\vec{\ell}$ via the charge-quadrupole interaction [see Fig. 1(c), top]. The core motion is thus no longer separable from the Rydberg-electron motion, which leads to a more complex dynamical behavior and a less regular structure of the Stark states. The distinguishing feature between the two categories is thus the zero vs nonzero value of N^+ and the role of the ion-core quadrupole in the latter case. In both cases, the calculations quantitatively reproduce the observed structures and can be used to derive the ion-core level structures in least-squares fits.

The ionization energies and the fine and hyperfine coupling constants obtained from these fits are presented in Table I and the corresponding residuals for the measurements at different electric fields and n values are displayed in Fig. 4. Typical error budgets for the cases of D_2 and H_2 are given in Tables SIII and SIV of Supplemental Material [56]. In each panel of Fig. 4, the different values of n for which spectra were measured are indicated by different colors, and for each n value the different data points correspond to different electric fields. The colored error bars represent statistical uncertainties (1σ). Their black extensions reflect systematic uncertainties in the quantum defects of the d series, which are the most strongly coupled to the f series and to the linear Stark manifolds. The shaded areas represent the final uncertainties encompassing both the contributions from the error bars of individual data points and their scatter [58]. The D_2^+ $X^+(1,0)$–D_2 $GK(2,2)$ and H_2^+ $X^+(1,2)$–H_2 $GK(2,0)$ ionization energies are determined at a relative accuracy better than 10^{-9}. The D_2^+ $X^+(0,0)$–D_2 $GK(0,2)$ ionization energy from Ref. [59] and the interval $GK(2,2)$-$GK(0,2)$ of 42 639 437.7(9) MHz derived here in a separate measurement can be combined to determine a value of 47 279 980.8(1.9) MHz for the fundamental vibrational frequency of D_2^+ [$X^+(1,0)$–$X^+(0,0)$], in perfect agreement with the more precise theoretical result of 47 279 981.589 8(12) MHz [60].

Precise experimental values for both the hyperfine coupling constant b_F of D_2^+ ($v^+ = 1, N^+ = 0$) [139.84(5) MHz] and the spin-rotation coupling constant c_e of H_2^+ ($v^+ = 1, N^+ = 2$) [39.62(11) MHz] are reported here for the first time and agree with theoretical values within the

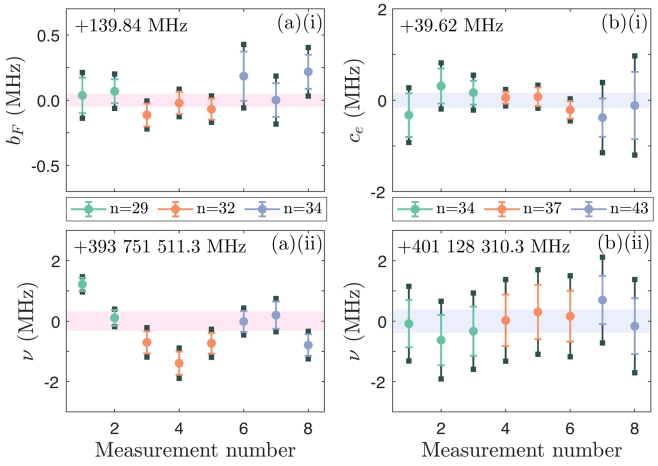


FIG. 4. Panels (a)(i) [(b)(i)]: residuals of the fitted hyperfine (spin-rotation) coupling constants of D_2^+ (H_2^+). Panels (a)(ii) [(b)(ii)]: residuals of the D_2^+ $X^+(1,0)$–$GK(2,2)$ and H_2^+ $X^+(1,2)$–$GK(2,0)$ intervals. The different data points at each value of n indicate the results obtained from measurements at different values of the electric field strength. The colored error bars show statistical uncertainties of the fitted parameters. Their black extensions represent systematic uncertainties of the calculations (see text for details). The colored areas indicate the final uncertainties.

experimental uncertainties, see Table I. The accuracy of the present hyperfine levels of *ortho*-D_2^+ $(v^+ = 1, N^+ = 0)$ even surpasses the accuracy in the hyperfine structure of the nonautoionizing $v^+ = 0, N^+ = 1$ level of *para*-D_2^+ derived from millimeter-wave spectra of transitions between high-n d and f Rydberg states under field-free conditions [61].

The excellent agreement between experimental and calculated spectra achieved here validates the theoretical approach presented in Ref. [49]. It enables the characterization of the structure and dynamics of high molecular Rydberg-Stark states with open-shell ion cores at an unprecedented level and the determination of ionic fine- and hyperfine-structure intervals in molecular ions. The strength of this approach lies in its applicability to any molecular ion that is accessible by photoionization.

Acknowledgments—We thank Dr. J.-Ph. Karr for useful advice on the theoretical treatment of the hyperfine structure of molecular hydrogen ions. We thank H. Schmutz and J. A. Agner for their technical assistance. This work is supported financially by the Swiss National Science Foundation (Grant No. 200021-236716) and the European Union's Horizon Europe Research and Innovation Programme and the Participating States (Grant No. 23FUN04 COMOMET).

Data availability—The data that support the findings of this article are not publicly available upon publication because it is not technically feasible and/or the cost of preparing, depositing, and hosting the data would be prohibitive within the terms of this research project. The data are available from the authors upon reasonable request.

[1] T. F. Gallagher, *Rydberg Atoms*, edited by A. Dalgarno, P. L. Knight, F. H. Read, and R. N. Zare, Cambridge Monographs on Atomic, Molecular and Chemical Physics (Cambridge University Press, Cambridge, 1994).

[2] R. F. Stebbings and F. B. Dunning, *Rydberg States of Atoms and Molecules* (Cambridge University Press, Cambridge, 1983).

[3] M. Germann, S. Patra, J.-Ph. Karr, L. Hilico, V. I. Korobov, E. J. Salumbides, K. S. E. Eikema, W. Ubachs, and J. C. J. Koelemeij, Three-body QED test and fifth-force constraint from vibrations and rotations of HD^+, Phys. Rev. Res. **3**, L022028 (2021).

[4] C. Delaunay, J.-P. Karr, T. Kitahara, J. C. J. Koelemeij, Y. Soreq, and J. Zupan, Self-consistent extraction of spectroscopic bounds on light new physics, Phys. Rev. Lett. **130**, 121801 (2023).

[5] V. I. Korobov, J.-P. Karr, and Z.-X. Zhong, Second-order corrections of orders $m\alpha^6$ and $m\alpha^6(m/M)$ to the spin-averaged energy in the HD^+ and H_2^+ ions, Mol. Phys. e2563023 (2025).

[6] S. Alighanbari, M. R. Schenkel, V. I. Korobov, and S. Schiller, High-accuracy laser spectroscopy of H_2^+ and the proton–electron mass ratio, Nature (London) **644**, 69 (2025).

[7] S. Schiller and J.-P. Karr, Prospects for the determination of fundamental constants with beyond-state-of-the-art uncertainty using molecular hydrogen ion spectroscopy, Phys. Rev. A **109**, 042825 (2024).

[8] M. Puchalski, J. Komasa, P. Czachorowski, and K. Pachucki, Nonadiabatic QED correction to the dissociation energy of the hydrogen molecule, Phys. Rev. Lett. **122**, 103003 (2019).

[9] N. Hölsch, M. Beyer, E. J. Salumbides, K. S. E. Eikema, W. Ubachs, Ch. Jungen, and F. Merkt, Benchmarking theory with an improved measurement of the ionization and dissociation energies of H_2, Phys. Rev. Lett. **122**, 103002 (2019).

[10] V. Patkóš, V. A. Yerokhin, and K. Pachucki, Complete $\alpha^7 m$ Lamb shift of helium triplet states, Phys. Rev. A **103**, 042809 (2021).

[11] G. Clausen and F. Merkt, Ionization energy of metastable ^{3}He ($2\,^3S_1$) and the alpha- and helion-particle charge-radius difference from precision spectroscopy of the np Rydberg series, Phys. Rev. Lett. **134**, 223001 (2025).

[12] P. J. Mohr, D. B. Newell, B. N. Taylor, and E. Tiesinga, CODATA recommended values of the fundamental physical constants: 2022, Rev. Mod. Phys. **97**, 025002 (2025).

[13] A. Facon, E.-K. Dietsche, D. Grosso, S. Haroche, J.-M. Raimond, M. Brune, and S. Gleyzes, A sensitive electrometer based on a Rydberg atom in a Schrödinger–cat state, Nature (London) **535**, 262 (2016).

[14] H. Zhang, Y. Ma, K. Liao, W. Yang, Z. Liu, D. Ding, H. Yan, W. Li, and L. Zhang, Rydberg atom electric field sensing for metrology, communication and hybrid quantum systems, Sci. Bull. **69**, 1515 (2024).

[15] C. Liang, C. Yang, W. Huang, and L. You, Exceptional point-enhanced Rydberg atomic electrometers, Phys. Rev. Lett. **136**, 053203 (2026).

[16] J. Nipper, J. B. Balewski, A. T. Krupp, B. Butscher, R. Löw, and T. Pfau, Highly resolved measurements of Stark-tuned Förster resonances between Rydberg atoms, Phys. Rev. Lett. **108**, 113001 (2012).

[17] S. Weber, C. Tresp, H. Menke, A. Urvoy, O. Firstenberg, H. P. Büchler, and S. Hofferberth, Calculation of Rydberg interaction potentials, J. Phys. B At. Mol. Opt. Phys. **50**, 133001 (2017).

[18] M. Stecker, R. Nold, L.-M. Steinert, J. Grimmel, D. Petrosyan, J. Fortágh, and A. Günther, Controlling the dipole blockade and ionization rate of Rydberg atoms in strong electric fields, Phys. Rev. Lett. **125**, 103602 (2020).

[19] Y. Jiao, J. Bai, R. Song, S. Bao, J. Zhao, and S. Jia, Electric field tuned dipolar interaction between Rydberg atoms, Front. Phys. **10**, 892542 (2022).

[20] P. Méhaignerie, Y. Machu, A. Durán Hernández, G. Creutzer, D. Papoular, J.-M. Raimond, C. Sayrin, and M. Brune, Interacting circular Rydberg atoms trapped in optical tweezers, PRX Quantum **6**, 010353 (2025).

[21] M. Peper, Y. Li, D. Y. Knapp, M. Bileska, S. Ma, G. Liu, P. Peng, B. Zhang, S. P. Horvath, A. P. Burgers, and J. D. Thompson, Spectroscopy and modeling of ^{171}Yb Rydberg states for high-fidelity two-qubit gates, Phys. Rev. X **15**, 011009 (2025).

[22] H. A. Bethe and E. E. Salpeter, *Quantum Mechanics of One- and Two-Electron Atoms* (Springer, Berlin, 1957).

[23] I. Doran, N. Hölsch, M. Beyer, and F. Merkt, Zero-quantum-defect method and the fundamental vibrational interval of H_2^+, Phys. Rev. Lett. **132**, 073001 (2024).

[24] M. L. Zimmerman, M. G. Littman, M. M. Kash, and D. Kleppner, Stark structure of the Rydberg states of alkali-metal atoms, Phys. Rev. A **20**, 2251 (1979).

[25] J. Grimmel, M. Mack, F. Karlewski, F. Jessen, M. Reinschmidt, N. Sándor, and J. Fortágh, Measurement and numerical calculation of rubidium Rydberg Stark spectra, New J. Phys. **17**, 053005 (2015).

[26] N. Šibalić, J. D. Pritchard, C. S. Adams, and K. J. Weatherill, ARC: An open-source library for calculating properties of alkali Rydberg atoms, Comput. Phys. Commun. **220**, 319 (2017).

[27] M. Peper, J. Deiglmayr, F. Merkt, C. Sanna, and H. B. van Linden van den Heuvell, Magic Rydberg–Rydberg transitions in electric fields, Phys. Rev. A **100**, 032512 (2019).

[28] S. Scheidegger, J. A. Agner, H. Schmutz, and F. Merkt, Metrology of Rydberg states of the hydrogen atom, Phys. Rev. A **108**, 042803 (2023).

[29] W. E. Ernst, T. P. Softley, and R. N. Zare, Stark-effect studies in xenon autoionizing Rydberg states using a tunable extreme-ultraviolet laser source, Phys. Rev. A **37**, 4172 (1988).

[30] P. F. Brevet, M. Pellarin, and J. L. Vialle, Stark effect in argon Rydberg states, Phys. Rev. A **42**, 1460 (1990).

[31] H. H. Fielding and T. P. Softley, Observation of the Stark effect in autoionizing Rydberg states of Ar with a multichannel quantum-defect analysis, J. Phys. B At. Mol. Opt. Phys. **25**, 4125 (1992).

[32] M. J. J. Vrakking, Role of core interactions and external perturbations in the autoionization of Xe, J. Phys. Chem. A **101**, 6761 (1997).

[33] C. Bordas, M. Broyer, J. Chevaleyre, and P. Labastie, Laser Stark spectroscopy of molecular Rydberg states, J. Phys. Colloques **48**, 647 (1987).

[34] C. Bordas and H. Helm, Stark effect in triatomic hydrogen Rydberg states, Phys. Rev. A **45**, 387 (1992).

[35] H. H. Fielding and T. P. Softley, Observation of the Stark effect in autoionizing Rydberg states of molecular hydrogen, Chem. Phys. Lett. **185**, 199 (1991).

[36] M. J. J. Vrakking, Lifetimes of Rydberg states in ZEKE experiments. III. Calculations of the dc electric field dependence of predissociation lifetimes of NO, J. Chem. Phys. **105**, 7336 (1996).

[37] Ch. Seiler, S. D. Hogan, and F. Merkt, Trapping cold molecular hydrogen, Phys. Chem. Chem. Phys. **13**, 19000 (2011).

[38] M. H. Rayment and S. D. Hogan, Quantum-state-dependent decay rates of electrostatically trapped Rydberg NO molecules, Phys. Chem. Chem. Phys. **23**, 18806 (2021).

[39] F. Munkes, M. H. Rayment, A. Trachtmann, F. Anschütz, E. Eder, P. Hengel, Y. Schellander, P. Schalberger, N. Fruehauf, J. Anders, R. Löw, T. Pfau, S. D. Hogan, and H. Kübler, High-resolution continuous-wave laser spectroscopy of long-lived Rydberg states in NO, J. Phys. Chem. Lett. **15**, 10171 (2024).

[40] D. A. Harmin, Hydrogenic Stark effect: Properties of the wave functions, Phys. Rev. A **24**, 2491 (1981).

[41] D. A. Harmin, Analytical study of quasidiscrete Stark levels in Rydberg atoms, Phys. Rev. A **30**, 2413 (1984).

[42] K. Sakimoto, Multichannel quantum-defect theory of the Stark effect, J. Phys. B At. Mol. Phys. **19**, 3011 (1986).

[43] K. Sakimoto, Influence of electric fields on highly excited states of H_2: Quantum-defect-theory approach, J. Phys. B At. Mol. Opt. Phys. **22**, 2727 (1989).

[44] H. H. Fielding and T. P. Softley, Observation of the Stark effect in autoionising Rydberg states of molecular hydrogen, Chem. Phys. Lett. **185**, 199 (1991).

[45] T. P. Softley, A. J. Hudson, and R. Watson, Multichannel quantum defect theory Stark effect calculation of autoionization lifetimes in high-n Rydberg states of Ar, N_2 and H_2, J. Chem. Phys. **106**, 1041 (1997).

[46] M. Grütter, O. Zehnder, T. P. Softley, and F. Merkt, Spectroscopic study and multichannel quantum defect theory analysis of the Stark effect in Rydberg states of neon, J. Phys. B **41**, 115001 (2008).

[47] P. Giannakeas, C. H. Greene, and F. Robicheaux, Generalized local-frame-transformation theory for excited species in external fields, Phys. Rev. A **94**, 013419 (2016).

[48] Ch. Jungen and G. Raseev, Spin-electronic-rotational frame transformation for photoionization and Rydberg spectra of diatomic molecules, Phys. Rev. A **57**, 2407 (1998).

[49] I. Doran, L. Jeckel, M. Beyer, Ch. Jungen, and F. Merkt, The Stark effect in molecular Rydberg states: Calculation of Rydberg-Stark manifolds of H_2 and D_2 including fine and hyperfine structures, Phys. Rev. A **113**, 062812 (2026).

[50] Ch. Jungen, *Molecular Applications of Quantum Defect Theory* (Institute of Physics Publishing, Bristol and Philadelphia, 1996).

[51] Ch. Jungen, Elements of quantum defect theory, in *Handbook of High-Resolution Spectroscopy*, edited by M. Quack and F. Merkt (John Wiley & Sons, Chichester, 2011), Vol. 1, pp. 471–510.

[52] P. Danev, D. Bakalov, V. I. Korobov, and S. Schiller, Hyperfine structure and electric quadrupole transitions in the deuterium molecular ion, Phys. Rev. A **103**, 012805 (2021).

[53] V. I. Korobov, L. Hilico, and J.-Ph. Karr, Hyperfine structure in the hydrogen molecular ion, Phys. Rev. A **74**, 040502(R) (2006).

[54] N. Hölsch, I. Doran, M. Beyer, and F. Merkt, Precision millimetre-wave spectroscopy and calculation of the Stark manifolds in high Rydberg states of para-H_2, J. Mol. Spectrosc. **387**, 111648 (2022).

[55] M. Beyer, N. Hölsch, J. A. Agner, J. Deiglmayr, H. Schmutz, and F. Merkt, Metrology of high-n Rydberg states of molecular hydrogen with $\Delta\nu/\nu = 2 \times 10^{-10}$ accuracy, Phys. Rev. A **97**, 012501 (2018).

[56] See Supplemental Material http://link.aps.org/supplemental/10.1103/5rsv-mb6x for the results of individual fits of Rydberg-Stark manifolds and typical error budgets.

[57] E. Tiesinga, P. J. Mohr, D. B. Newell, and B. N. Taylor, CODATA recommended values of the fundamental physical constants: 2018, Rev. Mod. Phys. **93**, 025010 (2021).

[58] E. Meister, *Grundpraktikum Physikalische Chemie: Theorie und Experimente* (vdf, Hochschul-Verlag an der ETH, Zürich, 2000).

[59] J. Hussels, N. Hölsch, C.-F. Cheng, E. J. Salumbides, H. L. Bethlem, K. S. E. Eikema, Ch. Jungen, M. Beyer, F. Merkt, and W. Ubachs, Improved ionization and dissociation energies of the deuterium molecule, Phys. Rev. A **105**, 022820 (2022).

[60] V. I. Korobov, L. Hilico, and J.-Ph. Karr, Fundamental transitions and ionization energies of the hydrogen molecular ions with few ppt uncertainty, Phys. Rev. Lett. **118**, 233001 (2017).

[61] H. A. Cruse, Ch. Jungen, and F. Merkt, Hyperfine structure of the ground state of *para*-D_2^+ by high-resolution Rydberg-state spectroscopy and multichannel quantum defect theory, Phys. Rev. A **77**, 042502 (2008).